APPENDIX B: Hydroclimatic reconstructions in the Lower Basin: Water year streamflow reconstruction of the Little Colorado River

by Kiyomi Morino and David Meko,
Laboratory of Tree-Ring Research, The University of Arizona

Table of Contents

B.1 Study Basin

The Little Colorado River drains an area of 68,600 km^2 (17.0 million acres) in northeastern Arizona and northwestern New Mexico and flows northwest across the Colorado Plateau to its confluence with the Colorado River (Figure B-1). Most of the tributaries of the Little Colorado are small ephemeral streams, and the main channel itself near the confluence with the Colorado River has no flow at times each year (Anderson and White 1986). Elevations in the basin range from less than 1000 m (3,280 ft) near the confluence of the Little Colorado and Colorado Rivers to more than 2800 m (9,180 ft) in the White Mountains of east-central Arizona.

B.2 Data

B.2.1 Hydrologic Data.

Monthly average streamflows for the Little Colorado River were downloaded from the U.S. Geological Survey (http://waterdata.usgs.gov/az/nwis/). Of a total of 16 gages on the river, 6 have data before 1948. The longest continuous record for a gage still in operation is the Little Colorado near Cameron, Arizona, which begins in June 1947. At the Cameron gage, the mean daily discharge for water years over the period of record is 6.17 cms (218 cfs) (USGS 2012a). The highest water year mean daily discharge was 31.91 cms (1127 cfs) in 1973; the lowest was 0.40 cms (14.1 cfs) in 2000. Average water year runoff is 194.77 mcm (157.9 kaf). Streamflow at the Cameron gage is affected by reservoirs upstream, but the degree of regulation is categorized as "negligible" (Anderson and White 1986). For calibration with tree rings we wanted a somewhat longer streamflow record, if possible including the notable Southwest wet year 1941 (Bradley et al. 1982). The Cameron record for water years 1948-2008 was therefore extended to water year 1936 by linear regression on streamflows 190 km (118 miles) upstream at Woodruff, Arizona ($R^2 = 0.70$, $N=61$, $p < 0.01$). The regression-extended water-year streamflows, 1936-2008, for the Colorado near Cameron are hereafter referred to as "observed streamflows." Observed and reconstructed streamflows for the Colorado River at Lees Ferry, Arizona, from Meko et al. (2007) were downloaded from NOAA's WDC for Paleoclimalogy (http://www.ncdc.noaa.gov/paleo/). Reconstructed streamflows for the Gila River were provided by D. Meko.

B.2.2 Precipitation Data

Precipitation variations were characterized with PRISM (Precipitation-elevation Regressions on Independent Slopes Model) data (Gibson et. al 2002). Monthly PRISM data, 1900-2010, for the continental US were downloaded from the PRISM site (http://prism.oregonstate.edu/products/). Data pertaining to the Little Colorado River basin were "clipped" from the larger dataset using a script written in MatLab ™. Volume of precipitation (MCM) over the entire basin was computed.

B.2.3 Hydroclimatology

The combined influence of winter cyclonic storms and the NAM are reflected in the bimodal distributions of monthly precipitation and streamflow (Figure B-2). Importance

of snowmelt is indicated by the lag between month of peak precipitation and peak flow. The streamflow response to summer rains also appears to be delayed, possibly because the July rainfall peak is largely spent in recharging soil moisture after the normally dry May and June.

Scatterplots of streamflow on seasonal-total precipitation over the whole basin for the period 1936-2008 suggest streamflow responds primarily to cool-season precipitation (Figure B-3). Correlation with water-year streamflow is equally high for precipitation summed over the water-year and over October-April (r=0.76 and r=0.79, respectively, N=70). Curvature in the scatter plots for the water-year and cool-season is consistent with an increase of runoff ratio with precipitation amount (e.g., Sellers 1965). Summer precipitation is essentially uncorrelated with annual streamflow (r =-0.08), despite contributing a substantial fraction of the annual precipitation (Figure B-2). This lack of correlation does not necessarily prove that summer precipitation is unimportant to annual streamflow. Elevated soil moisture from summer rains may facilitate the runoff efficiency of following cool-season precipitation. Moreover, importance of summer rainfall to streamflow may be masked partly by a weak tendency for negative correlation between summer and winter precipitation (r=-0.11, N=110, p=0.89).

Precipitation (*volP*) and streamflow (*Q*) are characterized by high interannual variability (Figure B-4). Generally dry conditions in the 1940s and 1950s give way to wetness in the late 1970s to early 1980s. Trend for 1936-2008, as described by a least-square-fit straight line of the hydrologic variable on water year, is positive for precipitation and negative for streamflow, but for neither series is the slope of the trend-line statistically significant. The trend in the ratio series *Q*/*volP* is negative but not significantly different from zero. Deletion of the two extremely wet years, 1941 and 1973, from the data makes a slight difference to this assessment in that the trend in *Q/volP* becomes weakly significant ($p<0.05$) (plot not shown).

B.2.4 Tree-Ring Data.

The starting tree-ring data for the study consisted of measured ring widths. These were obtained from the International Tree-Ring Data Bank (ITRDB) (http://www.ncdc.noaa.gov/paleo/treering.html), the Southwest Archaeology Project at the University of Arizona (personal communication, Gary Funkhouser), and collections by one of the authors (Meko) made for the Salt River Project (http://fp.arizona.edu/kkh/srp2.htm). The reconstruction generated in this study made use of 19 tree-ring chronologies, with the starting tree-ring data before screening consisted of ring widths from 30 sites in or near the basin (Figure B-1). Sites were selected with the criteria that the species be moisture-sensitive and the data cover at least the period 1550-1983. The 1550 cutoff ensured that all chronologies sampled the late-1500s megadrought (Schulman 1956; Meko et al. 1995; Stahle et al. 2000); the 1983 cutoff ensured a reasonably long period for calibration of streamflow with tree rings in the reconstruction model.

See *Hydroclimatic Reconstructions in the Lower Basin of the Colorado River, METHODS* for details regarding tree-ring data standardization.

B.3 Methods

Analysis of reconstructions utilized a variety of statistical tools. Correlation analysis and significance-testing of correlations follow Snedecor and Cochran (1989), with adjustment as needed for autocorrelation (Dawdy and Matalas 1964). Assessment of low-frequency fluctuations included smoothing by evenly-weighted moving averages (Panofsky and Brier 1958) and Gaussian filters (Mitchell et al. 1966). Covariation of the Little Colorado with: 1) the Colorado River and 2) the Gila River as a function of frequency was summarized by cross-spectral analysis (Bloomfield 2000). More details on this technique can be found in Meko and Woodhouse (2005).

B.3.1 Reconstruction Model

See *Hydroclimatic Reconstructions in the Lower Basin of the Colorado River, METHODS* for details regarding methods employed in single-site reconstructions.

B.4 Results and Discussion

B.4.1 Reconstruction modeling

Tree-Ring Chronology Development

The reduced set of 19 tree-ring chronologies passing the screening for sample depth and correlation with streamflow are listed in Table B-1. Their site locations are marked by shaded triangles on the map in Figure B-1. The common period is 1478-1983, though some extend to earlier and later years. Exploratory correlation analysis pointed to 1420 as a feasible start year for reconstruction. All chronologies were therefore truncated to start in either 1420 or the first year with adequate subsample signal strength (SSS>0.85). Descriptive statistics showed that the chronologies have near-zero autocorrelation and negative skew (Table B-2). Skew is significantly (p<0.01) negative for five chronologies. The near-zero autocorrelation is expected, as these are residual chronologies (Cook et al. 1990b).

Single-Site Reconstruction

The SSR models explain 20-47 percent of the variance of streamflow in the calibration period, which ranges in length from 48 to 73 years for the 19 sites (Table B-3). Calibration periods start with 1936, the first year of available streamflow data, but end in different years (1983 to 2008) depending on collection date of the chronology. All models have some skill of verification, as indicated by an RE-statistic above zero.

The final selected smoothing parameter, α , for the SSR models ranges from 0.40 to 0.85. The variation in selected α reflects differences in curvature of the statistical relationship between streamflow and tree-ring index where values closer to 1.0 indicate a more linear relationship between streamflow and tree-ring index.

Recalibration and Reconstruction

The percentage of streamflow variance explained by the models ranges from 46 percent for Model C to 66 percent for Model B (Table B-4). All three models have positive skill, reflected by positive RE statistics for cross-validation, and the root-mean-square error

increases only by a small amount (13-16 percent) from the calibration to the validation data.

Figure B-5 shows the loadings of each of the sites that comprise each of the three models. Model B was developed from the largest number of sites, eighteen (identified on Table B-3). Sites are generally evenly distributed around the perimeter of the basin, apart from a relative dearth of sites along the southeast boundary. This does not reflect an absence of sites (see Figure B-1) but rather that these sites did calibrate well with the instrumental streamflow record. Loadings for this model are relatively even across sites. Somewhat higher loadings occur for Navajo Mountain and Dinnebito Wash; whereas somewhat lower loadings occur for Eagle Creek and Black River. Models A and C are comprised of eight and seven sites, respectively. In both cases, these are located to the north and west edge of the basin. As with Model B, Dinnebito Wash figures strongly in Model A; whereas, Mesa Verde loads high for Model C.

Differences in tracking of observed streamflows since 1936 are evident in the time series plots of observed and reconstructed streamflow for the three models (Figure B-6). Differences are slight between Model A (8-site model) and Model B (17-site model). Model C gives a closer fit to 1952 and 1965 but does not track the wet year, 1941, as well as Models A and B. Similarly, Model C does a poor job in fitting the wet year, 1993.

Uncertainty

The validation statistics mirror the calibration R^2 in supporting the elevated accuracy of Model B over the other two models (Table B-4). Statistics for Model B are most relevant, as that model supplies the most years of reconstructed streamflows. The RMSE of cross-validation of Model B is 120.0 MCM, which is about two-thirds the standard deviation of observed streamflows for the 1936-83 calibration period of the model. There is some hint of dependence variance of reconstruction error on magnitude of reconstructed streamflow (Figure B-7). For positive residuals, the absolute value of residual appears to increase systematically with reconstructed streamflows (Figures B-7A,C). For example, the median absolute value of positive residual nearly doubles from the lowest to middle tercile of reconstructed streamflow (Figure B-7B). Assessment of such patterns is speculative, however, given the small sample size of the residuals.

B.4.2 Reconstructed streamflows

Annual streamflows

Annual reconstructed streamflows, 1420-2008, are plotted in Figure B-8A along with a baseline at the long-term median of 184 MCM (149 KAF) to facilitate identification of wet years and dry years. The annual reconstructed streamflows have a mean of 225 MCM (182 KAF), are positively skewed (skew =1.9, $p<0.01$), not significantly autocorrelated ($r_1=0.02$, $p>0.05$), and slightly wet relative to the observed streamflows, whose 1936-2008 mean is 206 MCM (167 KAF). The relative wetness is not surprising since the observed streamflows include one of the longest droughts (1950s) and do not begin until after the well-documented wet initial decades of the 20th century.

The 20th and early 21st centuries stand out in the long-term plot of annual streamflows for lack of very high flows, such as occurred in the mid-1850s and late 1500s. In the twentieth century, the frequency of years below the median in a 30-year sliding window peaks in the 1950s, with almost 2/3 of the years "dry", and contrasts the early 1900s when the frequency of dry years in a 30-yr sliding window was at an all-time low. (FigureB-8B). The highest frequency of dry years occurs in the late 1500s with more than two-thirds of the years "dry". A similarly high frequency of dry years also occurs in the mid-1400s.

Moving averages

Streamflow averaged over multi-year periods is relevant to water resources planning and management. Reconstructed streamflow anomalies for periods of length 5-50 years are summarized graphically in Figure B-9. This color-mapping of anomalies in running means uses the 1936-83 reconstructed mean as a baseline for "normal", but any other baseline would serve for illustrating relative conditions. The color pattern resembles flames, as tongues of red, indicating dry conditions, thin from the bottom to the top; the thinning reflects the tendency for moving averages to become closer to "normal" with increasing length of averaging period. The1950s emerges in Figure B-9 as one of about 6 relatively severe decadal-scale droughts: others occur in the mid-late 1400s, late 1500s, late 1600s, and 1700s. The relative severity of the 1950s drought, however, does not match the late 1500s drought with increases with window-width. Indeed, for window widths greater than about 25 years the 1500s and 1600s shows extended dry conditions compared to the period following 1700.

Covariation with Colorado River and Gila River

The Little Colorado streamflow reconstruction was compared to the Colorado River (Meko et al 2007) and the Gila River (Meko) reconstructions. Both the Colorado and Gila River reconstructions were truncated to match the shorter Little Colorado reconstruction. For both comparisons, cross-spectral analysis was conducted over the full common period, as well as over two sub-periods, from the beginning of the common period to 1700 and from 1700 to the end of the common period. Split-sample analysis of covariation was carried out to verify the stability of relationship over the full period.

Little Colorado River and Colorado River

Smoothed time series plots of the Little Colorado and Colorado reconstructions show close agreement in timing of low-frequency fluctuations (Figure B-10A). The 21-year Gaussian filter used to smooth the series in Figure B-10A emphasizes multi-decadal fluctuations. Joint drought, defined as smoothed series simultaneously in their lowest quartile, occurs 10 times in the last 500 years. The 1580s and 1660s are the longest of these joint droughts. A cross-spectral analysis of the two reconstructions supports strong agreement at all frequencies (Figure B-10B-D). The individual spectra are slightly low-frequency, with no significant peaks but relatively high variance at wavelengths 5-10 years (Figure B-10B, C). Coherency, analogous to correlation as a function of frequency, is significant across the full frequency-range of the spectrum (Figure B-10D). The phase spectrum shows no evidence of out-of-phase behavior in the two series (Figure B-10E).

The small departure from zero-phase at higher frequencies can be disregarded as having no practical importance as the corresponding offset in the time domain is less than a year.

Split-sample analysis of covariation indicates that the significant coherency between the two series occurs at different frequencies during different periods. Prior to 1700, significant peaks occur at frequencies with wavelengths between 5-10 years (Figure B-11A). After 1700, coherency peaks at low frequencies, i.e., wavelengths greater than 10 years, and at very high frequencies, i.e., wavelengths less than 5 years (Figure B-11B).

Little Colorado River and Gila River

Smoothed time series plots of the Little Colorado and Colorado reconstructions show very close agreement in timing of low-frequency fluctuations (Figure B-12A). Joint drought occurs 12 times in the last 500 years. As with the comparison of the Little Colorado and the Colorado, the 1580s and 1660s are the longest of these joint droughts. A cross-spectral analysis of the two reconstructions supports extremely strong agreement at all frequencies (Figure B-12B-D). The individual spectra are slightly low-frequency, with no significant peaks but relatively high variance at wavelengths 5-10 years (Figure B-12B, C). Coherency is significant across the full frequency-range of the spectrum (Figure B-12D). The phase spectrum shows no evidence of out-of-phase behavior in the two series (Figure B-12E).

In contrast to the comparison between the Little Colorado and Colorado Rivers, the split-sample analysis of covariation indicates that coherency between the Little Colorado and the Gila is relatively stable over time (Figure B-13A,B). For both periods of analysis, before and after 1700, coherency is significant across the spectrum with the exception of very low frequencies prior to 1700 (Figure B-13A).

B.5 Conclusions

The time series of reconstructed streamflows of the Little Colorado reveals several interesting features of long-term variation of the Little Colorado river. In the 20Th century, the most severe drought occurred in the 1950s. The low flows during this period are particularly emphasized by the generally wetter conditions immediately preceding it in the 1920s. It was the late 1500s, however, that hosted the most severe drought of this reconstruction. Interestingly, the highest reconstructed streamflow also occurs in the late 1500s.

Covariation of the Little Colorado with the Colorado River and Gila River indicate strong similarities, especially with the latter. This is to be expected from a hydroclimatological standpoint as the major runoff producing regions for both basins are located in relatively close proximity. Moreover, in both cases, water year streamflow is dominated by winter precipitation which tends to be highly spatially homogeneous across the region. From a statistical standpoint, some of the similar patterns in covariation may be attributed to a partial overlap in the chronologies used to generate both of these reconstructions.

TABLES

Table B-1. List of site chronologies.

N[1]	Site[2]	Species[3]	Location[4] Lat	Lon	El(m)	Period[5]
1	Dry Creek	PIED	34.9	-111.8	1377	1626-1986
2	Eagle Creek	PIED	33.5	-109.5	1694	1639-1987
3	Ord Mountain	PIPO	33.9	-111.4	2133	1567-1987
4	Sit. Gravel Pit	PIPO	34.3	-109.9	2072	1622-1986
5	Slate Mountain	PIPO	35.5	-111.8	2194	1590-1986
6	Baldy Peak	PSME	34.0	-109.6	2940	1556-1983
7	Black River	PSME	33.8	-109.3	2434	1565-2008
8	Paria Group I[6]	PSME	37.6	-112.2	2500	1259-2010
9	Spider Rock	MIX	36.1	-109.3	1890	1290-1990
10	Paria Group II[7]	PIED	37.4	-111.9	2000	1406-2010
11	Ditch Canyon	PSME	37.0	-107.8	2036	1610-2008
12	Dinnebito Wash	PIED	36.2	-110.5	1920	1390-1983
13	Mesa Verde	PSME	37.2	-108.5	2042	480-2008
14	Kane Springs	PIED	37.5	-109.9	1966	1276-1988
15	Navajo Mountain	PIED	37.0	-110.8	2286	1269-1989
16	Pueblita Canyon	PSME	36.7	-107.3	2005	1643-2009
17	Red Butte	PIED	35.8	-112.1	1920	1415-2005
18	Tsegi & Betatakin	PSME	36.7	-110.5	2043	863-2008
19	El Malpais NM	PSME	35.0	-108.1	2423	-136-1992

1 Site number
2 Site name
3 Species code: PIED is *Pinus edulis*; PIPO is *Pinus ponderosa*; PSME is *Pseudotsuga menzeisii*.
4 Latitude and longitude in decimal degrees, elevation in m above sea level
5 Start and end year of chronology, after trimming as described in text
6 Paria Group I: Bryce Canyon and Upper Henderson
7 Paria Group II: Coal Bench, Lower Henderson, Round Valley & Skutumpah Rd2

Table B-2. Chronology basic statistics

N	Length[1]	Mean	Stdev	Skew[2]	r(1)[3]	Replication and Common Signal[4] #Cores	SSS	EPS
1	335(224)	1.000	0.252	0.00	-0.02	4- 25	0.89	0.86-0.97
2	300(153)	1.002	0.252	-0.41**	-0.03	4- 20	0.86	0.83-0.96
3	408(175)	1.002	0.201	-0.28*	0.00	3- 19	0.87	0.80-0.94
4	347(217)	1.001	0.165	0.13	0.03	3- 24	0.88	0.86-0.98
5	329(158)	0.997	0.227	-0.18	0.02	4- 37	0.88	0.86-0.98
6	362(173)	0.999	0.038	0.22	-0.05	9- 24	0.90	0.80-0.93
7	411(154)	0.999	0.185	-0.01	-0.04	4- 85	0.88	0.87-0.99
8	611(166)	0.998	0.112	-0.55**	-0.07	7- 71	0.90	0.89-0.98
9	590(158)	1.001	0.217	-0.25*	-0.03	5- 52	0.86	0.83-0.98
10	439(150)	0.999	0.192	-0.54**	-0.09	5- 83	0.88	0.86-0.99
11	337(155)	0.997	0.252	-0.06	-0.01	3- 51	0.87	0.85-0.99
12	574(164)	1.000	0.265	-0.18	-0.04	3- 54	0.90	0.89-0.99
13	609(152)	0.998	0.204	-0.13	-0.05	19- 96	0.95	0.94-0.99
14	589(178)	1.001	0.219	-0.44**	-0.06	4- 51	0.88	0.87-0.99
15	590(188)	0.994	0.261	-0.17	-0.07	5- 25	0.94	0.92-0.98
16	352(168)	0.998	0.236	0.35**	-0.03	3- 51	0.87	0.86-0.99
17	528(162)	1.004	0.221	-0.19	-0.01	5- 92	0.85	0.84-0.99
18	609(153)	0.999	0.204	-0.22*	-0.04	14-179	0.96	0.96-1.00
19	605(155)	0.996	0.257	0.09	-0.04	17- 38	0.99	0.97-0.99

1 Length of site chronology, with minimum segment length in parentheses
2 Skewness (*,** denote significance at 0.05, 0.01 level)
3 First-order autocorrelation (*,** denote r(1) significantly different from zero at 0.05, 0.01 level)
4 Range in number of cores, minimum value of subsample signal strength, and range in expressed population signal

Table B-3. Summary of single-site loess models.

	Calibration[2]			Validation[3]		
N[1]	Period	α	V	RMSE	RE	RMSE	Model[4]
1	1936-1986	0.50	0.30	147.3	0.18	162.9	B
2	1936-1987	0.50	0.30	145.9	0.19	159.5	
3	1936-1987	0.40	0.20	156.2	0.06	172.3	B
4	1936-1986	0.65	0.39	137.7	0.30	149.8	B
5	1936-1986	0.60	0.27	150.2	0.14	166.4	B
6	1936-1983	0.50	0.43	135.8	0.30	154.1	B
7	1936-2008	0.80	0.23	150.6	0.16	159.4	BC
8	1936-2008	0.50	0.29	144.2	0.13	162.4	ABC
9	1936-1989	0.65	0.40	133.4	0.32	145.3	AB
10	1936-2008	0.60	0.25	148.2	0.19	156.6	BC
11	1936-2008	0.75	0.23	150.4	0.16	159.3	C
12	1936-1983	0.85	0.47	131.5	0.41	141.0	AB
13	1936-2008	0.30	0.35	137.9	0.19	156.8	ABC
14	1936-1988	0.65	0.25	150.0	0.18	159.7	AB
15	1936-1989	0.60	0.31	143.9	0.24	153.7	AB
16	1936-2008	0.80	0.23	150.6	0.15	160.6	BC
17	1936-2005	0.65	0.26	150.1	0.21	157.0	B
18	1936-2008	0.70	0.31	142.0	0.28	148.0	ABC
19	1936-2004	0.65	0.20	156.0	0.13	165.2	AB

1 Site number, as used in Table 1
2 Calibration statistics: N=period for estimation of loess curve,
α=loess smoothing parameter,V=variance-explained decimal fraction,
RMSE=root-mean-square error of calibration
3 Validation statistics from leave-1-out cross-validation:
RE=reduction of error statistic, RMSE=root-mean-square error
4 Subperiod reconstruction groups each chronology is used in (see Table 4)

Table B-4. Summary of sub-period reconstruction models.

			Calibration[4]			Validation[5]	
N[1]	Period[2]	p[3]	α	V	RMSE	RE	RMSE
A	1410-1983	8	0.40	0.65	106.8	0.54	124.1
B	1658-1983	17	0.45	0.66	104.6	0.57	120.0
C	1672-2008	7	0.35	0.46	126.3	0.32	143.0

1 Sub-period model number
2 Starting and ending years of sub-period
3 Number of chronologies
4 Calibration statistics: α=loess smoothing parameter, V=variance-explained decimal fraction, RMSE=root-mean-square error of calibration
5 Validation statistics from leave-1-out cross-validation: RE=reduction of error statistic, RMSE=root-mean-square error

FIGURES

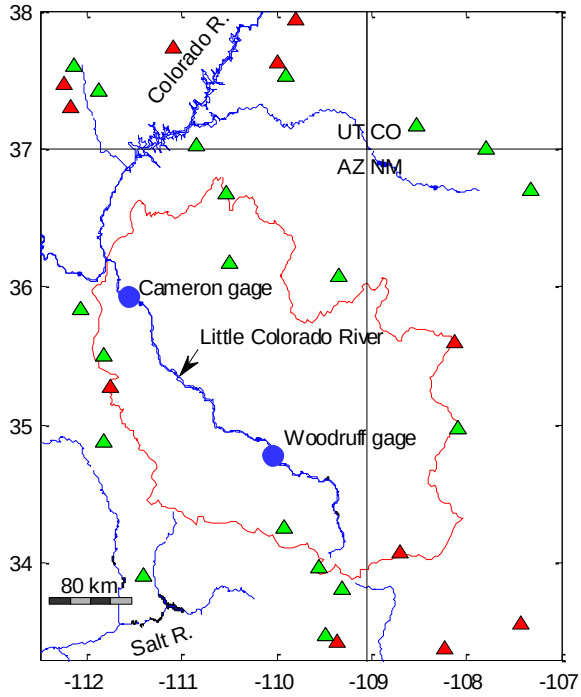

Figure B-1. Site map.

Map showing the Little Colorado River watershed and tree-ring site locations. Tree-ring sites that passed screenings for sample depth and correlations with streamflow are denoted by green triangles. Tree-ring sites that did not pass screenings are denoted by red triangles.

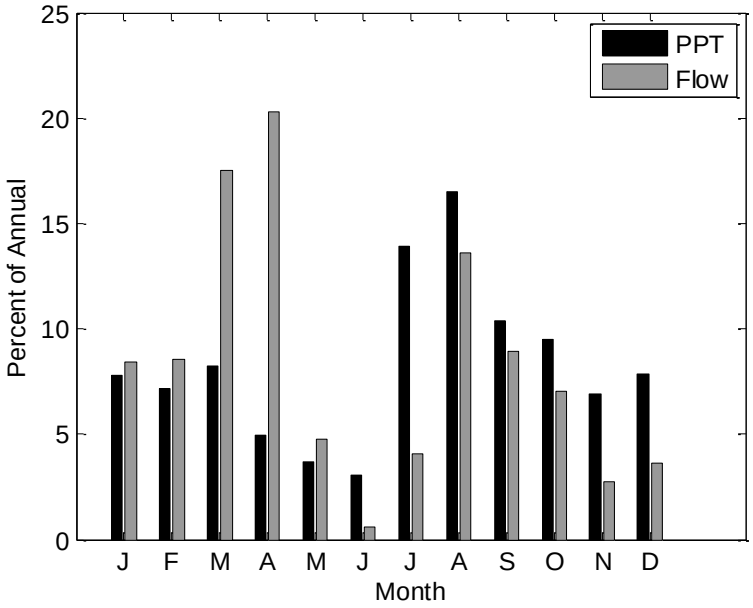

Figure B-2. Monthly basin precipitation and streamflow.

Bar charts summarizing annual distribution of monthly basin precipitation and streamflow. Streamflow data is from the gage at Cameron, Arizona. Precipitation data is from PRISM. Period of analysis is 1948-2008.

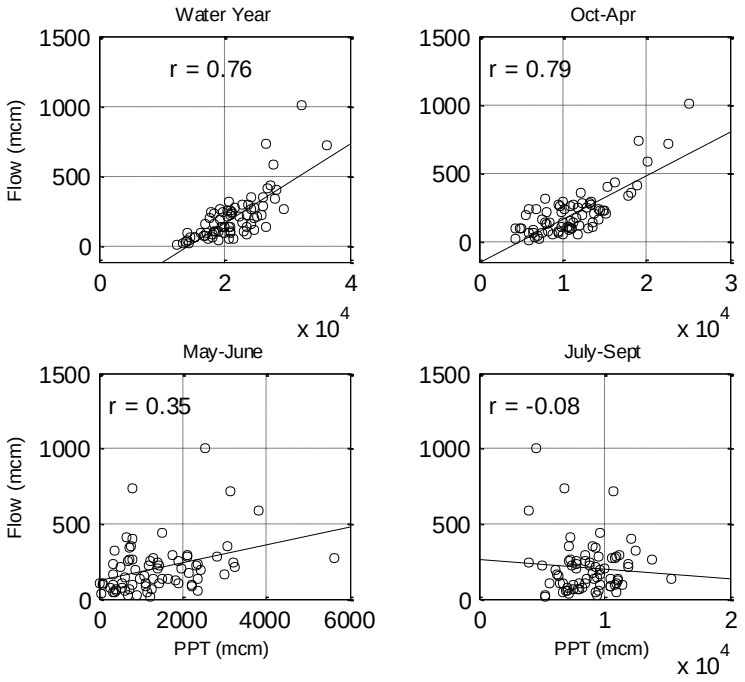

Figure B-3. Scatterplots of annual streamflow on seasonal precipitation.

Streamflow is for gage at Cameron, Arizona, extended to 1936 from gage at Woodruff. Precipitation is total volume of water year precipitation over the entire basin. Precipitation data is from PRISM. Period of analysis is 1936-2008.

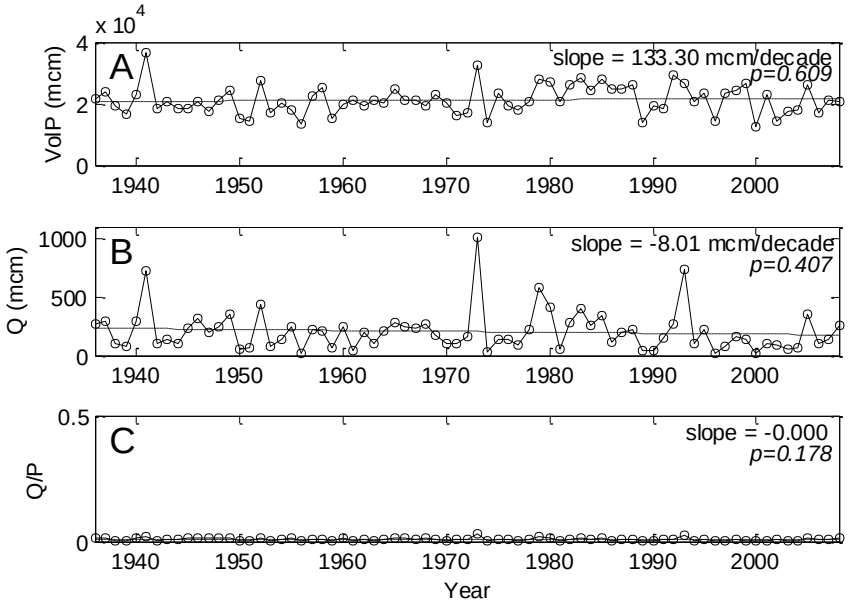

Figure B-4. Time trends in precipitation, streamflow, and the ratio of streamflow to precipitation.

(A) Total volume of precipitation over the Little Colorado River watershed for water year. (B) Streamflow on the Little Colorado River at Cameron for water year in million cubic meters (MCM). (C) Ratio of streamflow to precipitation. Least squares fit straight line for 1936-2008 is plotted for each series, and slope and its significance are annotated.

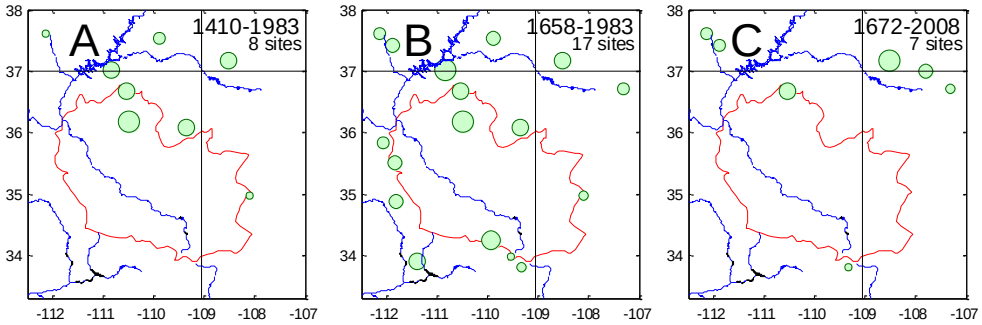

Figure B-5. PC loadings.

Tree-ring site locations for sub-period reconstruction models. Models A, B and C coded as in Tables 4. Symbol sizes reflect magnitude of loadings of sites on PC#1 of SSRs.

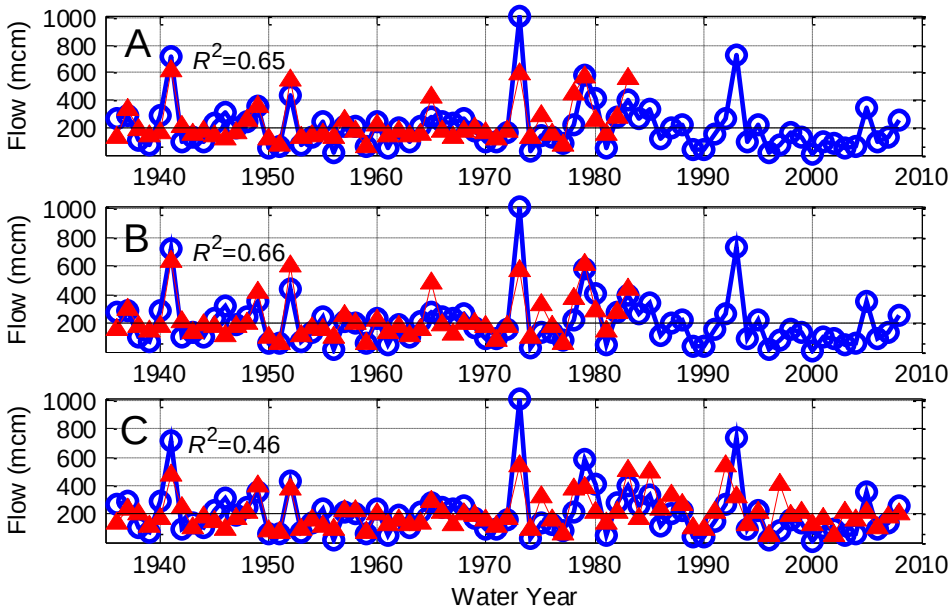

Figure B-6. Agreement of observed and reconstructed streamflow.

Agreement of observed and reconstructed streamflows for three sub-period models (as coded in Table 4). Annotated at upper left is the variance explained by the model. Horizontal line is the observed mean streamflow for the period, 1936-2008.

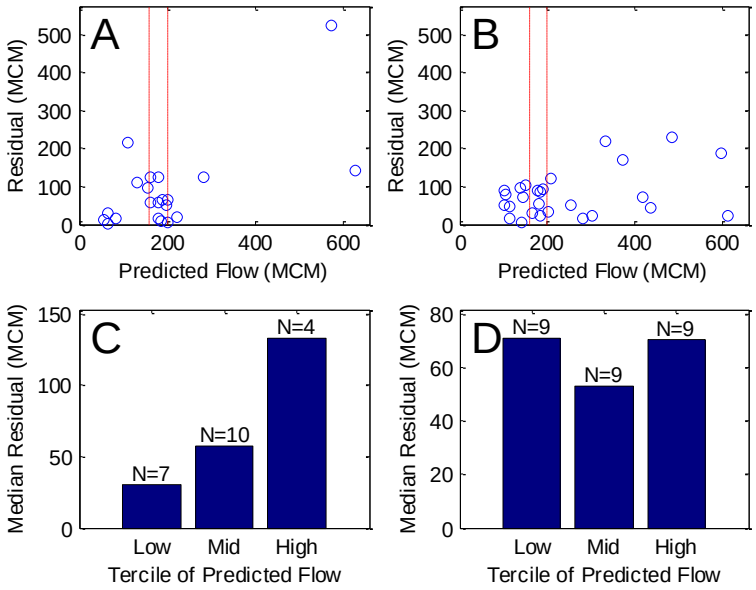

Figure B-7. Estimated reconstruction uncertainty.

Estimated reconstruction uncertainty for Model B. Terciles of reconstructed (predicted) streamflow, 1936-1983, are marked by vertical dashed lines in A and B. (A) Positive cross-validation residuals as function of predicted streamflow. (B) Absolute value of negative cross-validation residuals as function of predicted streamflow. (C) Median positive cross-validation residual for different terciles of reconstructed streamflow. (D) Median of absolute values of negative cross-validation residuals for terciles of reconstructed streamflow.

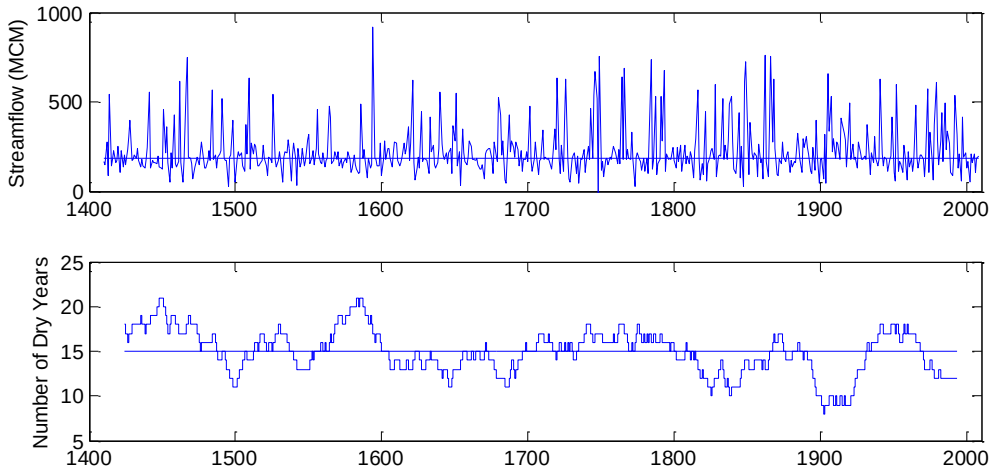

Figure B-8. Time plots of annual reconstructed streamflow.

Time plots of annual reconstructed years and dry-year frequency. (A) Reconstructed flows, 1410-2008, and dry year threshold (horizontal line) at median. (B) Frequency of dry years in centered 30-year moving window. The median reconstructed streamflow is 184 MCM (149 KAF), or 82 percent of the long-term mean, 225 MCM (182 KAF). Horizontal line in (B) is expected number of dry years in 30-year window.

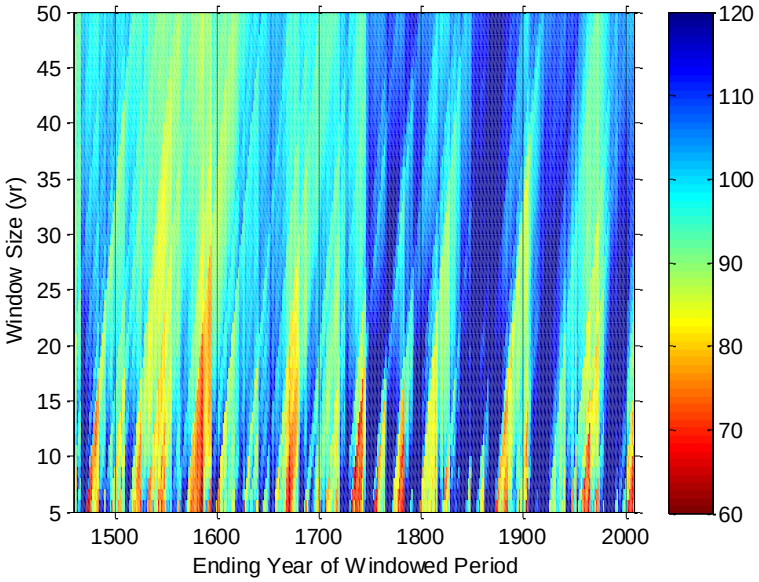

Figure B-9. Color-mapped running means of reconstructed streamflow.

Running means of length 5, 6, …50 years ending in years 1545-2010 are mapped as a percentage of the 1930-2010 reconstructed mean. Color mapping is truncated at 60 and 120 percent of the mean: streamflows lower than 60 percent are mapped as the darkest red and streamflows greater than 120 percent as the darkest blue.

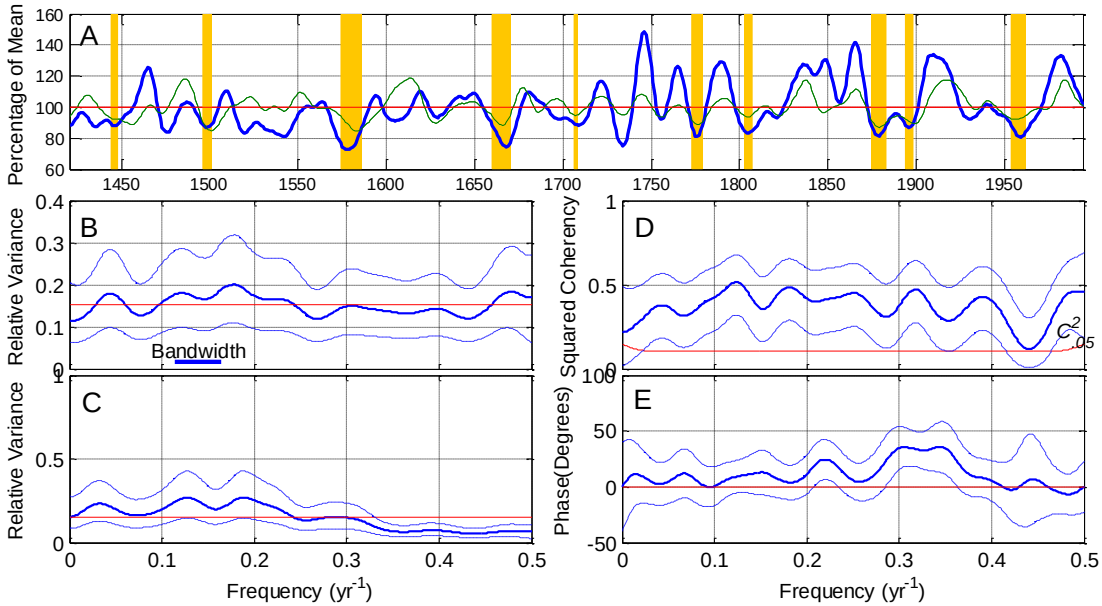

Figure B-10. Covariation of Little Colorado and Colorado River reconstructed streamflows, 1410-2005

(A) Smoothed reconstructed streamflow series as percentage of long-term mean. Intervals with smoothed series simultaneously below 0.25 quantile shaded. Thick blue line is Little Colorado River; thin green line is Colorado River. (B) Spectrum of Little Colorado. (C) Spectrum of Colorado. (D) Coherency spectrum from cross-spectral analysis of Little Colorado and Colorado. (E) Phase spectrum from the cross-spectral analysis. Smoothing in (A) by 21-year Gaussian filter. Confidence intervals (dashed) on spectral and cross-spectral plots are 95%. Line labeled $C^2_{.05}$ is threshold for rejection of null hypothesis of zero coherency at 0.05 α-level.

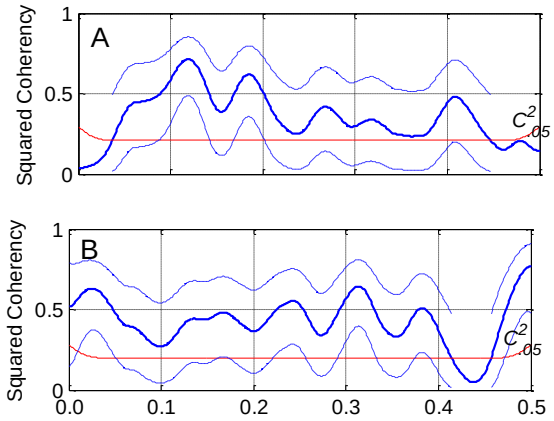

Figure B-11. Split-sample coherency analysis.

(A) Coherency spectrum of cross-spectral analysis the Little Colorado and Colorado Rivers for period, 1410 – 1700; (B) Coherency spectrum of cross-spectral analysis the Little Colorado and Colorado Rivers for period, 1700 – 2005.

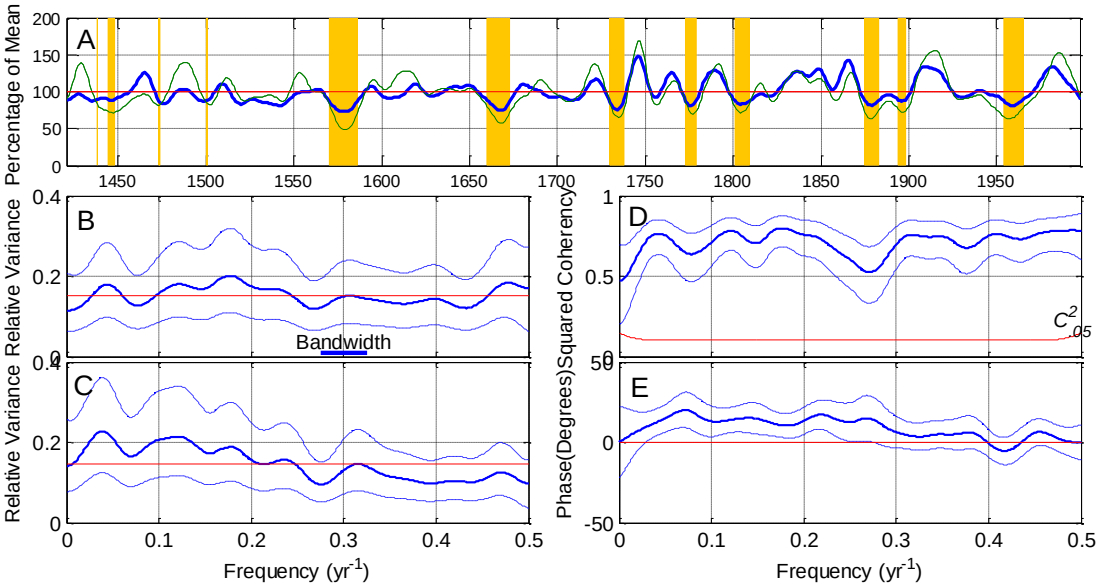

Figure B-12. Covariation of Little Colorado and Gila River reconstructed streamflows, 1410-2008

(A) Smoothed reconstructed streamflow series as percentage of long-term mean. Intervals with smoothed series simultaneously below 0.25 quantile shaded. Thick blue line is Little Colorado River; thin green line is Gila River. (B) Spectrum of Little Colorado. (C) Spectrum of Gila . (D) Coherency spectrum from cross-spectral analysis of Little Colorado and Gila Rivers. (E) Phase spectrum from the cross-spectral analysis. Smoothing in (A) by 21-year Gaussian filter. Confidence intervals (dashed) on spectral and cross-spectral plots are 95%. Line labeled $C^2_{.05}$ is threshold for rejection of null hypothesis of zero coherency at 0.05 α-level.

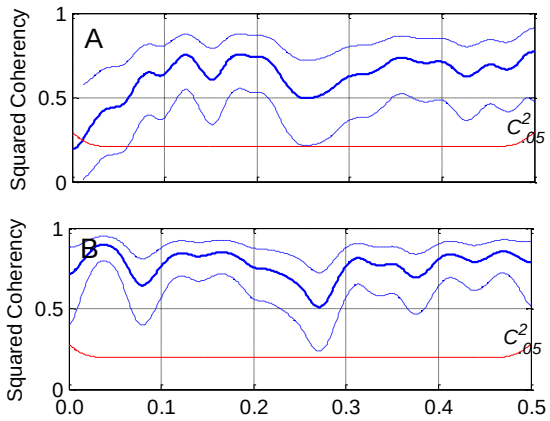

Figure B-13. Split-sample coherency analysis.

(A) Coherency spectrum of cross-spectral analysis the Little Colorado and Gila Rivers for period, 1410 – 1700; (B) Coherency spectrum of cross-spectral analysis the Little Colorado and Gila Rivers for period, 1700 – 2008.